Evaluation of Simplified Model for Rapid Identification and Control Development of IPM Traction Machines

Khoa D. Hoang, *Senior Member, IEEE*, Panagiotis Lazari, Kais Atallah, Jeff G. Birchall, and Stuart D. Calverley

***Abstract*— The paper presents an evaluation of simplified model considering only *q*-axis current effects on parameters for rapid identification and control development of interior permanent magnet (IPM) traction machines. It is shown that identification of the simplified model is simple and easy to be implemented. It is demonstrated that in the low-speed region with maximum torque per ampere (MTPA) control, due to the flat segment around the MTPA point of the relevant constant torque over current magnitude curve, MTPA operation could still be achieved using the simplified model. It is shown that in the field-weakening (FW) region where effects of parameter mismatch resulting in a higher than expected voltage magnitude could be mitigated via a voltage feedback (FB) loop, torque-speed performance still could be obtained with a reduction in the torque-speed boundary together with up to 1.5% machine efficiency difference. Thus, the simplified model could be considered at the earlier stage of identification and control development as a rapid solution to quickly test and validate IPM machine design/manufacture when validation of the complex model considering effects of both *dq*-axis currents is highly time-consuming. The simplified model is validated via measurement on a high-speed high-power (15000rpm, 120kW) IPM traction machine.**

***Index Terms*— Control development, field-weakening (FW) control, maximum torque per ampere (MTPA) control, interior permanent magnet (IPM) machine, traction applications.**

I. Introduction

DUE to its high torque density, high efficiency, and high field weakening (FW) operation ability [1], interior permanent magnet (IPM) machine is often employed under torque control mode for traction application [2]. Since IPM machines are well-known for their nonlinear characteristics [3]-[4], good knowledge of machine parameters is highly essential for validation of magnetic design and manufacture.

Theoretically, *dq*-axis inductances and PM flux linkage of IPM machines are often described as a function of *dq*-axis currents [3]-[12] and therefore, parameter identification often involves injection of different *dq*-axis current sets into the tested machine, data collection (voltages, currents, torque), and post-measurement processing. However, in practice, IPM machine identification is complicated and measurement errors resulting in mismatch issue are inevitable. In [5], for parameter identification, current and stepwise voltage on different *dq*-axis were simultaneously applied to the tested machine with locked rotor. Based on measured voltages and currents, information of relevant flux linkages and self-/cross-coupling inductances could be extracted. However, due to the locked rotor, voltage space harmonics are neglected and therefore, parameter estimation errors are inevitable. In [6], a dyno was utilized to control the tested machine at a constant speed and resistor-capacitor (RC) low-pass filter together with fast Fourier transform were employed to compute *dq*-axis flux linkages from measured voltages, currents, and phase angles referred to the rotor position. However, unavoidable phase lag and attenuation error may highly affect the identification accuracy. In [7], *dq*-axis flux linkages were computed from measured/estimated *dq*-axis voltages and currents of the tested machine. Again, accuracy of rotor position information is highly essential for this proposed technique. In [8], measurement from a torque transducer was utilized to extract PM flux linkage and the different value between *dq*-axis inductances. However, a lot of assumptions was required for the proposed method. A dynamic method without requiring a dyno for speed control was presented in [9] where *dq*-axis flux linkages were determined from the measured *dq*-axis voltages and currents obtained during acceleration and breaking of the tested machine in two rotational directions. However, very high sampling rate measurement equipment/data-loggers are required for collecting and processing measured data. Self-identification techniques were presented in [10] and [11] where high-frequency *dq*-axis currents [10] or DC/AC signals [11] were applied to the tested machine for parameter determination. Since rotor of the tested machine under these methods must be managed at standstill with signal injection, these methods are significantly difficult to be implemented. In [12], a study on IPM machine performance using simplified model was introduced. However, only preliminary results were presented.

Khoa D. Hoang, Panagiotis Lazari, and Kais Atallah are with the Department of Electronic and Electrical Engineering, the University of Sheffield, Sheffield S1 3JD, U.K. (email: k.hoang@sheffield.ac.uk; p.lazari@sheffield.ac.uk; k.atallah@sheffield.ac.uk). (*Corresponding author: Khoa D. Hoang.*)

Jeff G. Birchall and Stuart D. Calverley are with the Hybrid Drives Department, Magnomatics ltd, Sheffield S2 5BQ, UK (email: j.birchall@magnomatics.com; s.calverley@magnomatics.com).

Control developments for IPM traction machine were presented in [3], [4], and [13]-[17] where maximum torque per ampere (MTPA) control is often utilized in the low-speed operation region. Also in [4], it was demonstrated that the segment around the MTPA operation point of the relevant constant torque over current magnitude curve is considerably flat and therefore, variation of *dq*-axis currents over this flat segment may not significantly affect the MTPA achievement for the obtained torque. On the other hand, it was shown in [4] and [16] that effects of parameter mismatch resulting in a higher than expected voltage magnitude could be mitigated by a voltage FB loop in the FW operation region. In addition, thermal effects on IPM machine performances were studied in [17] where it was demonstrated that in the high-torque/high-speed operation region, rotor temperature variation may result in parameter mismatch leading to compromising the tested machine performance.

For validation of traction application, traction machine operations are often demonstrated over different driving cycles [1], [12] with the majority of operating points are located within the low-speed operation region. Therefore, at the earlier stage of identification and control development of IPM traction machine, when full parameter validation is highly time-consuming (e.g. long tested time required to rectify measurement errors resulting in parameter mismatches), a simplified machine model with acceptable accuracy, especially at low-speed operation region, for a rapid solution to quickly test and validate machine design together with manufacture is essential. This is the main focus of the paper.

The paper presents an evaluation of rapid parameter identification and control development using simplified IPM machine model considering only effects of *q*-axis current on machine parameters. The proposed technique is validated by measurements on a high-speed high-power (15000rpm, 120kW) IPM traction machine. It is demonstrated that identification of the simplified model is simple, easy to be implemented, and could be quickly completed within a short-period of time to avoid the issue of rotor temperature variation [17]. It is shown that in the low-speed operation region with MTPA control, due to the flat segment around the MTPA point of the relevant constant torque over current magnitude curve, MTPA operation could still be achieved for the tested machine with the simplified model. It is demonstrated that in the field-weakening (FW) region where effects of parameter mismatch resulting in a higher than expected voltage magnitude could be mitigated via a voltage FB loop, torque-speed performance still could be obtained for the tested machine under simplified model with a reduction in torque-speed boundary and up to 1.5% machine efficiency difference. Therefore, the simplified model could be considered as a rapid solution to quickly test and validate magnetic design together with manufacture for IPM traction machine with acceptable accuracy, especially at low-speed operation region.

The paper content is as follows. Mathematical model for IPM machine and control development are discussed in section II. Simplified model of IPM machine together with parameter identification are introduced in section III. IPM machine performances under the simplified and complex *dq*-axis current reference LUTs are compared and discussed in section IV. Measurement validation for IPM machine with the complex and simplified models is presented in section V. Some conclusions are discussed in section VI.

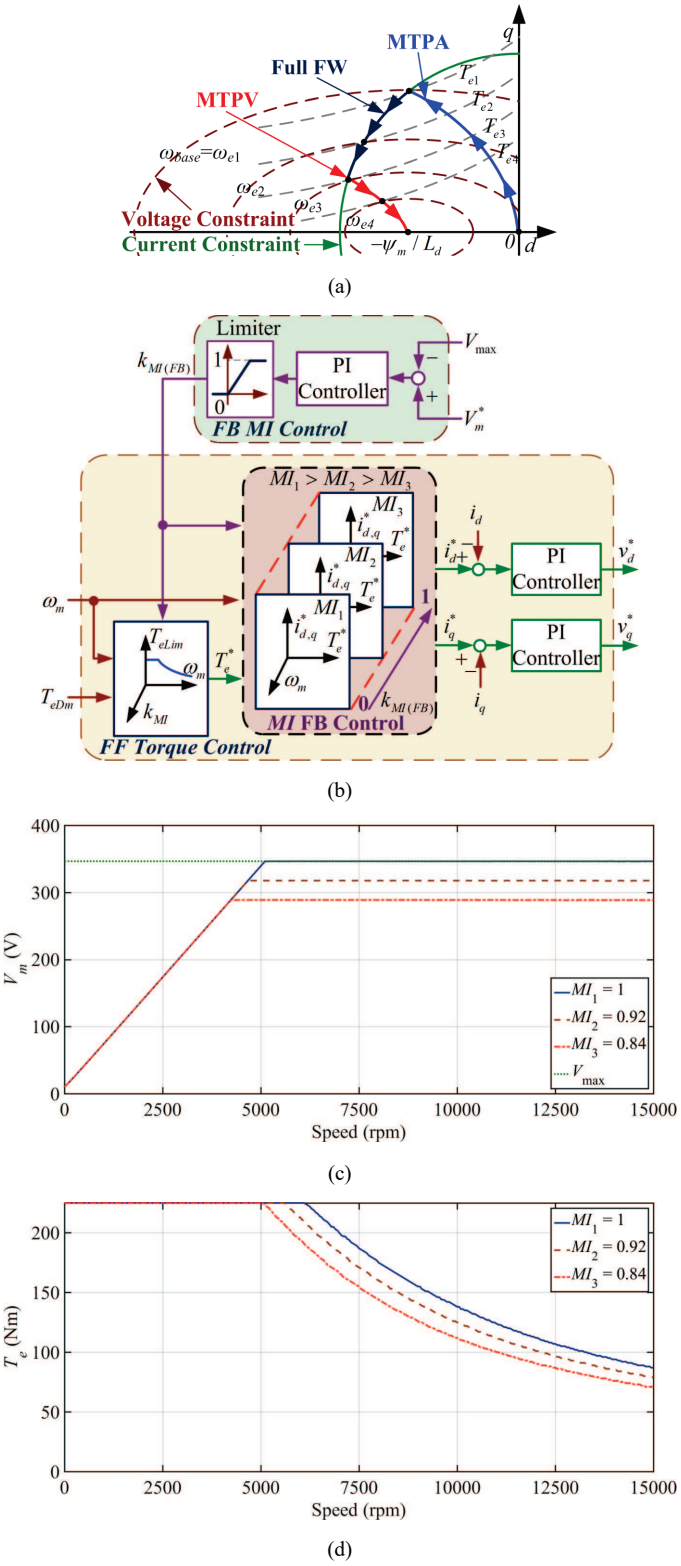

Fig. 1. Control of IPM traction machine. (a) Operation regions. (b) Control methodology [4], [12]. (c) Maximum voltages under different MI targets. (d) Maximum torques under different MI targets.

II. IPM Machine Model and Control Development

A. IPM Machine Model for Control Development

According to [1], [3], the mathematical model in *dq*-axis reference for IPM machines in the steady state is as follows.

$$v_d = R_s i_d - \omega_e \psi_q \;;\; v_q = R_s i_q + \omega_e \psi_d \quad (1)$$

$$\psi_d = L_d i_d + \psi_m \;;\; \psi_q = L_q i_q \quad (2)$$

$$T_e = (3/2) p[\psi_m + (L_d - L_q) i_d] i_q \quad (3)$$

where $v_{d,q}$, $i_{d,q}$, $\psi_{d,q}$, $L_{d,q}$ are the transformed (dq) voltages, currents, stator flux-linkages, and stator inductances, respectively; ω_e is the stator electrical frequency; R_s is the stator resistance; T_e is the machine torque; ψ_m is the PM flux linkage; p is the number of pole pairs.

The machine current is limited by a maximum value $I_{\max}$ associated with the selected cooling method [17].

$$I_m = \sqrt{i_d^2 + i_q^2} \le I_{\max} \quad (4)$$

For a selected modulation technique, maximum achievable phase voltage $V_{\max}$ is expressed in (5) where V_{dc} is the DC-link voltage; k_m is the modulation factor [3].

$$V_m = \sqrt{v_d^2 + v_q^2} \le V_{\max} \;;\; V_{\max} = k_m V_{dc} \quad (5)$$

B. IPM Machine Operation Regions

Operation regions for IPM machine is illustrated in Fig. 1(a) [1]. As can be seen, in the low-speed operation region where machine voltage is still lower than the maximum achievable voltage $V_{\max}$, the MTPA operation could be employed considering the current limitation (4) [3]-[4].

In the high-speed operation region, under a demanded torque, *dq*-axis current references are selected to maintain both demanded torque and voltage limit (5) as shown in the full FW operation region in Fig. 1(a). It is noted that the maximum current $I_{\max}$ is still achievable in the full FW region. However, when the machine speed increases, for a given maximum achievable voltage (5), there is an associated maximum achievable torque regardless of the current constrain $I_{\max}$ and the operation region limited by this maximum achievable torque is named as maximum torque per voltage (MTPV) [1], [12].

It is noted that the *dq*-axis inductances and the PM flux linkage values in (1) to (3) are nonlinear and often described as a function of *dq*-axis currents [3]-[11].

C. Control Development for IPM Traction Machine

For control development of IPM traction machine, the control methodology in Fig. 1(b) using predefined *dq*-axis current reference look-up tables (LUTs) with demanded torque and rotor speed as inputs are utilized [4], [12]. As can be seen, in the FW operation region, to mitigate effects of machine parameter mismatch and maintain the machine voltage at the maximum achievable value, a voltage feedback (FB) loop together with *dq*-axis current reference LUTs under lower modulation index (MI) targets are employed, Fig. 1(c). By way of example, the voltage FB MI control loop is activated when the voltage reference V_m^* is higher than the maximum achievable voltage $V_{\max}$ leading to a positive output value $k_{MI(FB)}$ to control relevant *dq*-axis current references for a lower modulation index target (i.e. from MI_1 to MI_2). As a result, the voltage reference V_m^* is reduced until it is equal to $V_{\max}$. It is noted that the voltage FB adjustment for a lower modulation index target could compromise the maximum achievable torque, Fig. 1(d). It is also noted that the control method in Fig. 1(b) as well as the voltage FB loop performance was well described in [4] and [16] and therefore not being detailed in this paper to avoid duplication.

The selected control technique in Fig. 1(b) is developed for a high-speed high-power (15000rpm, 120kW) IPM traction machine with single-layer magnet rotor (see Fig. 19(a) in the Appendix), Fig. 2, of which specifications are presented in Table I and further details could be found in [12]. For control development, first, the machine nonlinear parameters were generated from FEA and validated via measurement [5]-[11], Fig. 3. Then, for a given torque-speed operation point, variation of *dq*-axis currents from zero to their maximum values considering voltage and current limitations is implemented to find proper sets of *dq*-axis currents satisfying the demanded torque. Finally, the optimum *dq*-axis current set is selected for achieving the demanded torque with minimum current magnitude.

Figs. 4(a) and 4(b) present determined *dq*-axis current reference LUTs for the tested IPM machine. As can be seen, the control development method can satisfy MTPA control by obtaining demanded torque with minimum required current magnitude; full FW operation by considering both current and voltage boundary; and MTPV operation by considering voltage boundary. In addition, constant torque over current magnitude curves together with MTPA trajectory of the tested IPM traction

(a)

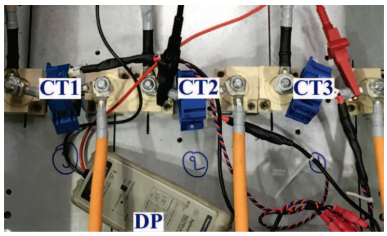

(b)

Fig. 2. IPM traction machine test-rig. (a) Test-rig with dyno and torque transducer. (b) Measurement equipment.

TABLE I

SPECIFICATIONS OF TESTED IPM TRACTION MACHINE - SINGLE-LAYER MAGNET ROTOR [12]

Continuous / Peak torque (Nm)	112.5 / 225
Peak current (A) / DC-link voltage (V)	340 / 600
Base / Maximum speed (rpm)	5850 / 15000
Number of pole pair	4

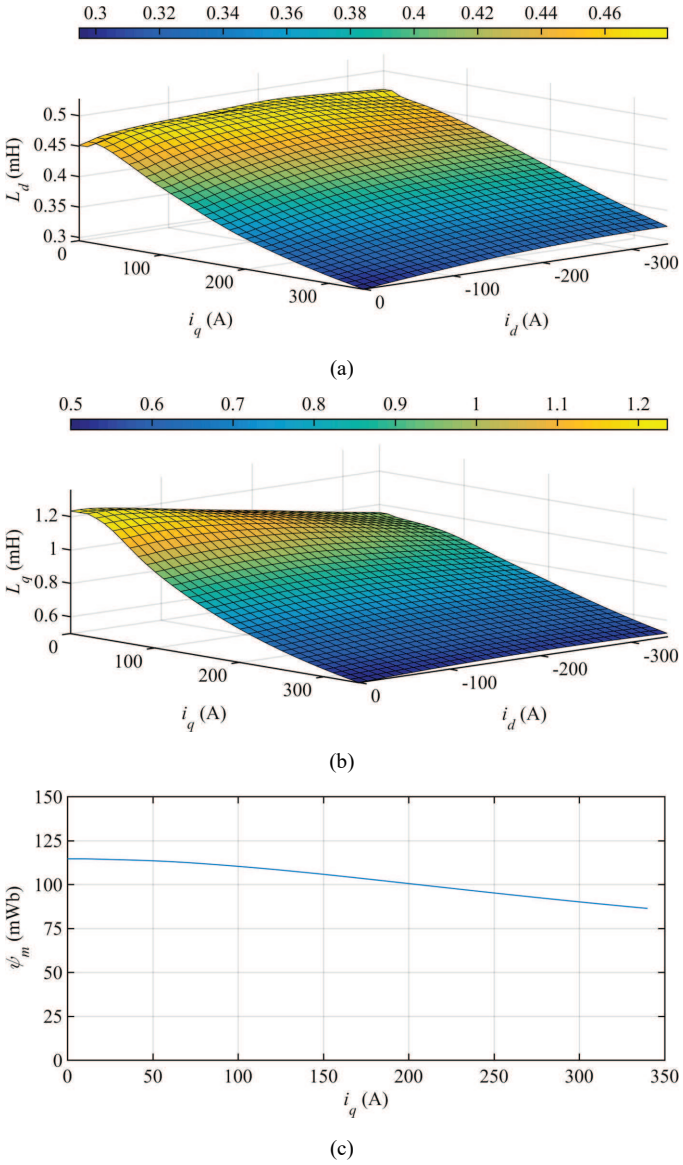

Fig. 3. Complex model of tested IPM machine [12]. (a) *d*-axis inductance. (b) *q*-axis inductance. (c) PM flux linkage.

machine are depicted in Fig. 4(c). As can be seen, the segments around the MTPA operation points of the relevant constant torque over current magnitude curves are considerably flat and therefore, variation of *dq*-axis currents over these flat segments may not significantly affect the MTPA achievement for the obtained torques. Similar phenomenon was introduced and discussed in details in [4]. It is noted that parameter identification for the machine complex model in Fig. 3 is complicated with unavoidable measurement errors [5]-[11] which may require a considerable amount of time to rectify. Thus, a simplified model with acceptable accuracy is proposed in the next section for rapid parameter identification and control development of IPM traction machine, when full parameter validation is highly time-consuming.

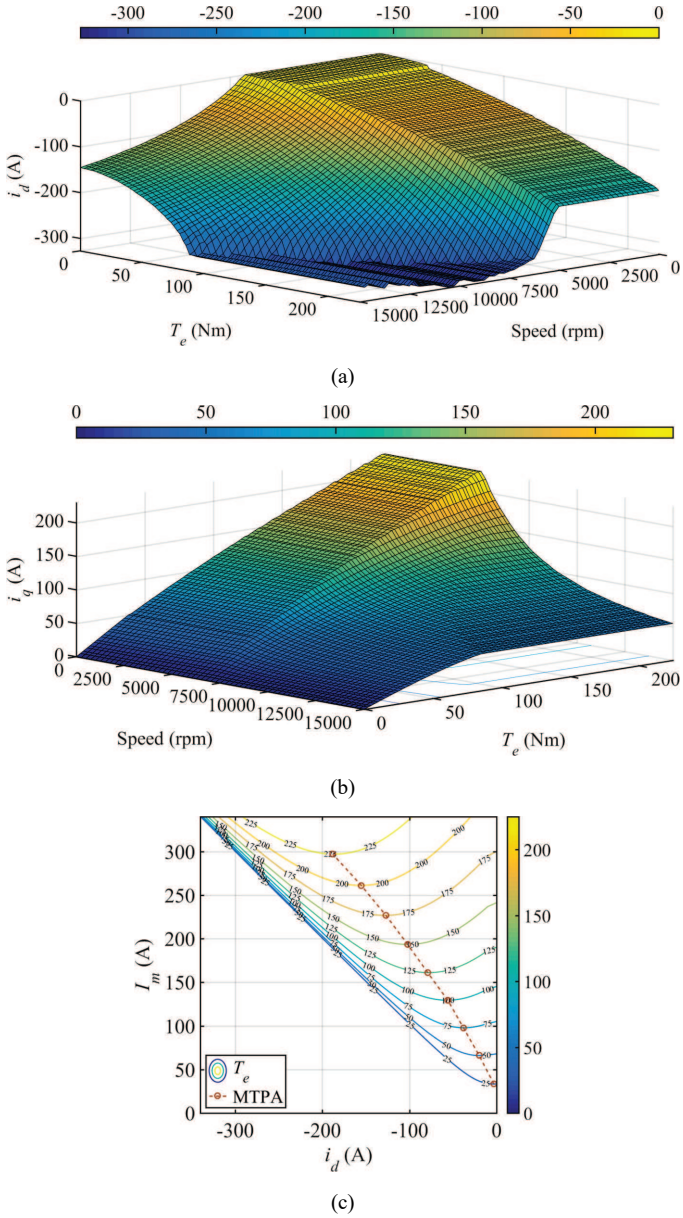

Fig. 4. Complex model current reference LUTs. (a) *d*-axis current reference. (b) *q*-axis current reference. (c) Constant torque over current magnitude curves and MTPA trajectory.

III. Simplified IPM Machine Model for Rapid Parameter Identification and Control Development

A. Simplified Model for IPM Machines

For IPM machine, saturation effect is mainly contributed by the *q*-axis current whereas cross-coupling effect is caused by both *dq*-axis current components. As can be seen in Fig. 3, the nonlinear characteristic of the tested IPM machine is predominantly affected by the *q*-axis current. Hence, by considering only the *q*-axis current effect on machine parameter, a simplified machine model with rapid parameter identification could be defined.

B. Parameter Identification of Simplified Model

The test-rig arrangement for parameter identification of

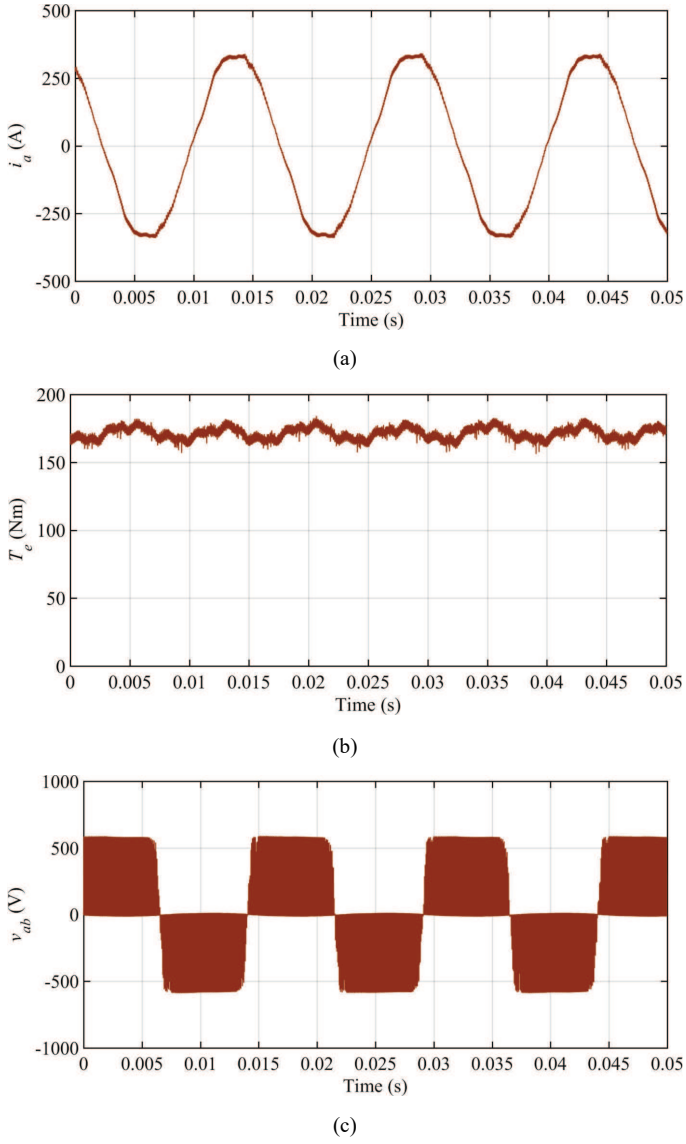

Fig. 5. Measurements for simplified model identification of tested IPM machine at 1000rpm, $i_d = 0$A, $i_q = 340$A. (a) Current waveform. (b) Torque waveform. (c) Line-to-line voltage waveform.

simplified model is illustrated in Fig. 2(a) where the dyno is operated at a constant speed as 1000rpm and the high-precision torque transducer (KISTLER 4503B) is employed for torque measurement. On the other hand, phase current and line-to-line voltage is respectively measured by current transducer (CT) (LEM LF310S) and voltage differential probe (DP) (KEYSIGHT N2891A) at the machine terminals, Fig. 2(b). Further details of the test-rig could be found in the section V. During the parameter identification, the tested machine is controlled by an inverter for variation of *dq*-axis currents and measurements for parameter identification is presented in Fig. 5 including phase current, torque, and line-to-line voltage. In addition, stator winding temperature is also sensed by installed thermistors. Based on the measurement in Fig. 5, the simplified model could be determined by two separate steps. In the first step, PM flux linkage together with *q*-axis inductance as a function of *q*-axis current are determined. Then, *d*-axis inductance as a function of *q*-axis current is defined in the

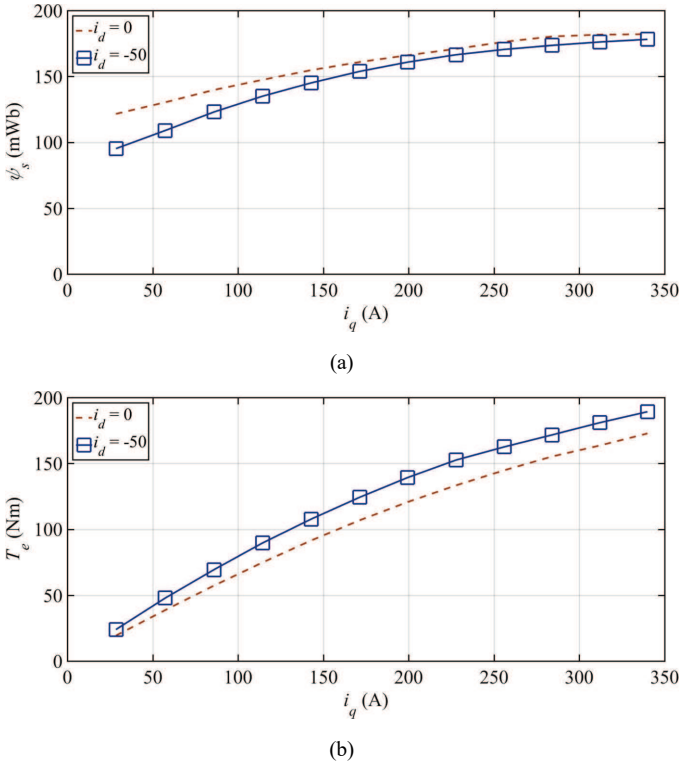

Fig. 6. Measurments for simplified model identification of tested IPM machine. (a) Measured flux linkage. (b) Measured torque.

second step.

In the first step, with the dyno operating at a constant speed (1000rpm), *d*-axis current of the tested machine is kept at zero while *q*-axis current is varied up to the maximum value $I_{\max}$ (340A) by setting on the inverter. Using measured torque and voltage, the PM flux linkage ψ_m and stator flux magnitude ψ_s as a function of *q*-axis current could be computed using (6) and (7) where $R_{s(T)}$ is the stator winding resistance as a function of stator winding temperature T. Results from (6) and (7) are used to calculate the *q*-axis inductance as shown in (8). It is noted that the measured current in Fig.5 is used to crosscheck the demanded current setting on the inverter.

$$\psi_m = T_e / (3pi_q / 2) \tag{6}$$

$$\psi_s \cong (V_m - I_m R_{s(T)}) / \omega_e \tag{7}$$

$$L_q = (\sqrt{\psi_s^2 - \psi_m^2}) / i_q \tag{8}$$

In the second step, effects of *d*-axis inductance on the tested machine torque could be obtained by applying a small *d*-axis current value to the tested machine while varying the *q*-axis current up to the maximum current value ($I_{\max}$) by the inverter. By assuming that the *q*-axis inductance obtained from (8) is not affected by the small *d*-axis current applied, the torque difference ΔT_e between the first and second step contributing by the machine reluctant torque component in (9) is utilized together with the obtained *q*-axis inductance for calculating the *d*-axis inductance showing in (10). It is noted that the *d*-axis inductance could also be computed from the stator flux obtained under constant *d*-axis current using (2) and (7). It is also noted that the selected *d*-axis current value should be high enough to produce a sufficient reluctant torque using in (9) but it should

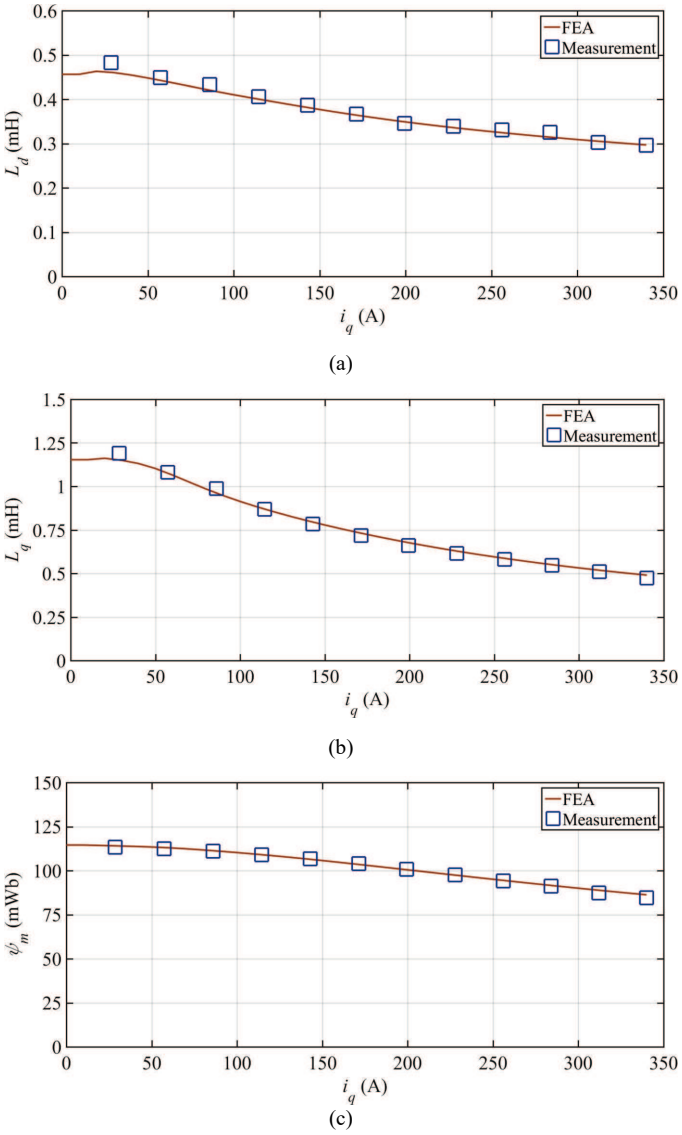

Fig. 7. Simplified model identification of tested IPM machine. (a) *d*-axis inductance. (b) *q*-axis inductance. (c) PM flux linkage.

also be small enough for its cross-coupling effects on the *q*-axis inductance to be neglected. In practice, this value could be selected as around 10 to 20% of the machine symmetrical short-circuit current value at steady state $I_{sc} = -\psi_m / L_d$ [the center point of voltage ellipse constraints, Fig. 1(a)]. For the tested IPM machine with MTPV operation, absolute value of I_{sc} is smaller than the $I_{\max}$, Fig. 1(a). Therefore, a small *d*-axis current value around 10 to 15% of the $I_{\max}$ could be initially selected for the second step. This initial value should be amended later for being about 10 to 20% of I_{sc} (computed from L_d obtained in this step and ψ_m derived from the previous step).

$$\Delta T_e = T_{e(2nd)} - T_{e(1st)} \tag{9}$$

$$L_d = [(2\Delta T_e)/(3pi_d i_q)] + L_q \tag{10}$$

Measured results of parameter identification with simplified model for the tested IPM machine are presented in Fig. 6 where a *d*-axis current as -50A (15% of machine maximum current $I_{\max}$ as 340A and 18% of I_{sc} computed as -270A) is selected for the second step. As can be seen in Figs. 3(a) and 3(b), the cross-coupling effect on the *q*-axis inductance causing by the applied *d*-axis current as -50A is not significant and could be neglected. Fig. 7 shows good agreement between the machine parameters determined from measurements for the simplified model and FEA. As can be seen, the identification for the simplified model is simple, easy to be implemented, and could be quickly completed within a short-period of time to avoid measurement errors due to rotor temperature variation [17].

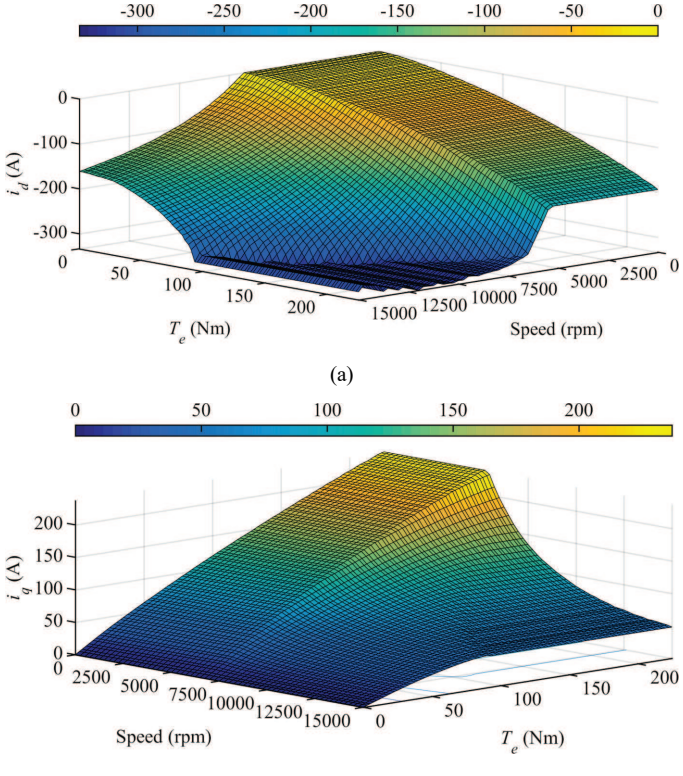

Fig. 8. Simplified model-based *dq*-axis current reference LUTs for tested IPM machine. (a) *d*-axis current reference. (b) *q*-axis current reference.

C. *Control Development using Simplified Model*

Based on the obtained parameters for the simplified model of the tested IPM traction machine in Fig. 7, relevant *dq*-axis current reference LUTs for the selected control technique in Fig. 1(b) are generated and depicted in Fig. 8. In the next section, a comparative study of the tested IPM machine performance under the complex model-based current reference LUTs, Fig. 4, and the simplified model-based current reference LUTs, Fig. 8, is presented to evaluate the simplified model as a rapid solution to quickly test and validate machine magnetic design together with manufacture with acceptable accuracy, especially at low-speed operation region.

IV. Comparative Performance Analysis between Simplified and Complex Models

In the section, comparative study of the tested traction machine performance under the complex model-based current reference LUTs, Fig. 4, and the simplified model-based current reference LUTs, Fig. 8, is presented to evaluate the simplified model. For comparative purpose, two remarks are expressed as

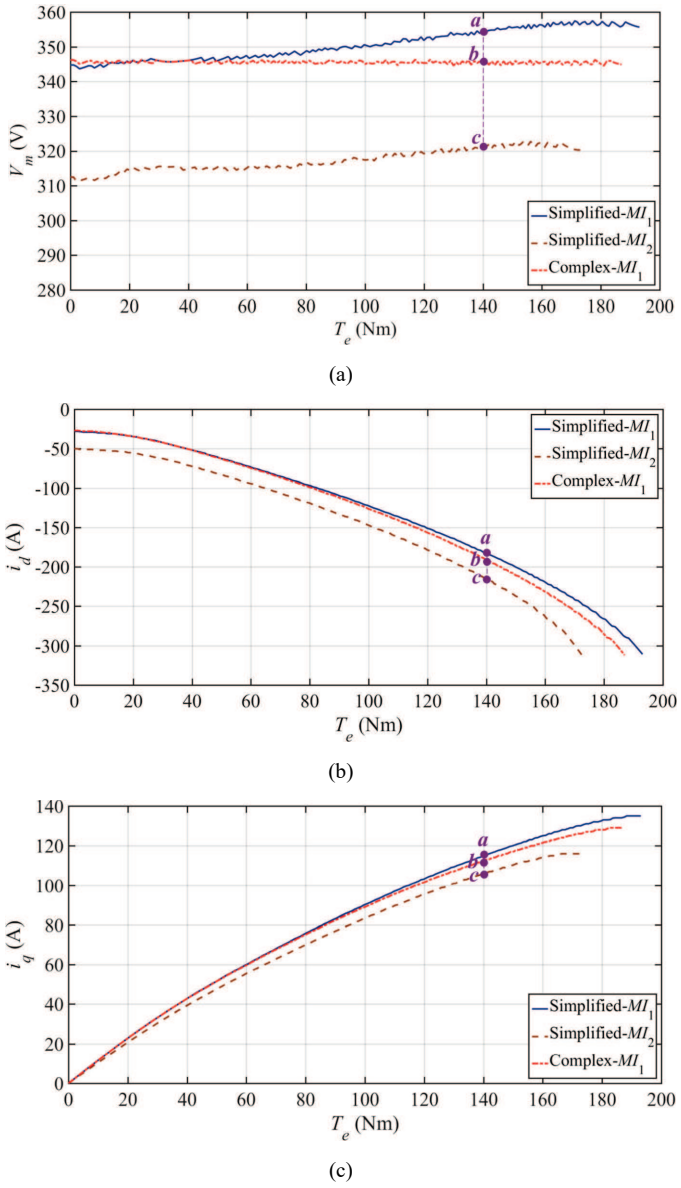

Fig. 9. Voltage and current for obtained torque at 7500rpm of tested IPM machine in FW operation under first scenario. (a) Voltage magnitude. (b) *d*-axis current. (c) *q*-axis current.

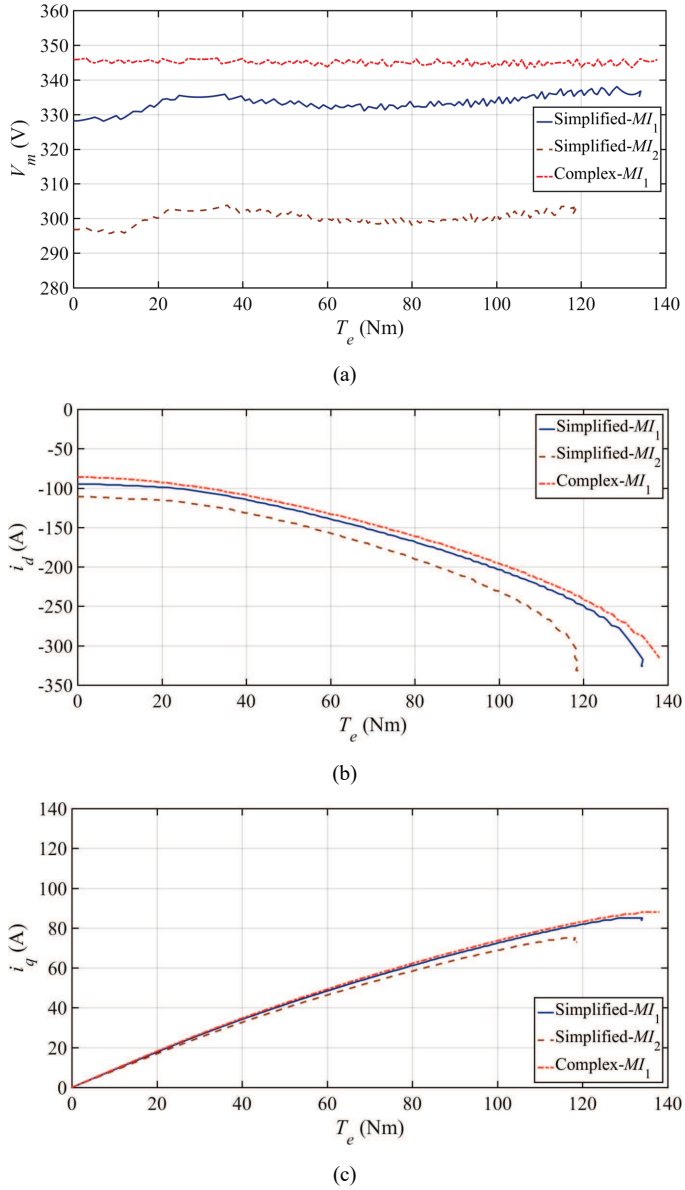

Fig. 10. Voltage and current for obtained torque at 10000rpm of tested IPM machine in FW operation under scecond scenario. (a) Voltage magnitude. (b) *d*-axis current. (c) *q*-axis current.

follows.

Remark 1: By applying non-ideal current reference LUTs under the simplified model in Fig. 8 to the tested IPM traction machine, for a given demanded torque, mismatch torque obtained in comparison with the ideal case is inevitable. However, for traction application where traction machine is often operated under torque control mode with the driver acting on demanded torque [3]-[4], **the expected torque could be finally obtained via demanded torque adjustment by the driver**.

Remark 2: In the FW operation region, while the obtained torque is managing by the driver, when the machine voltage is higher than its maximum limitation (5) due to the employment of the non-ideal current reference LUTs, Fig. 8, **the voltage FB control loop in Fig. 1(b) will be activated to adjust the *dq*-axis current references for a lower modulation index target until the machine voltage is maintained at its maximum achievable value** (the voltage FB loop performance was well described in [4], and [16] and therefore not being detailed in this paper to avoid duplication). However, employment of non-ideal current reference LUTs may not maximize the torque-speed boundary in the FW region for the simplified model and therefore, a lower than expected torque-speed boundary may be unavoidable.

Based on the *Remark 1* and *Remark 2*, **machine efficiency over obtained torque-speed operation is essential for a fair performance comparison between the simplified model and the complex model** with the simplified model acting as a rapid solution to quickly test and validate magnetic design together with manufacture of the tested IPM traction machine.

To demonstrate the effects of the voltage FB loop in the FW operation region, voltage magnitude together with *dq*-axis

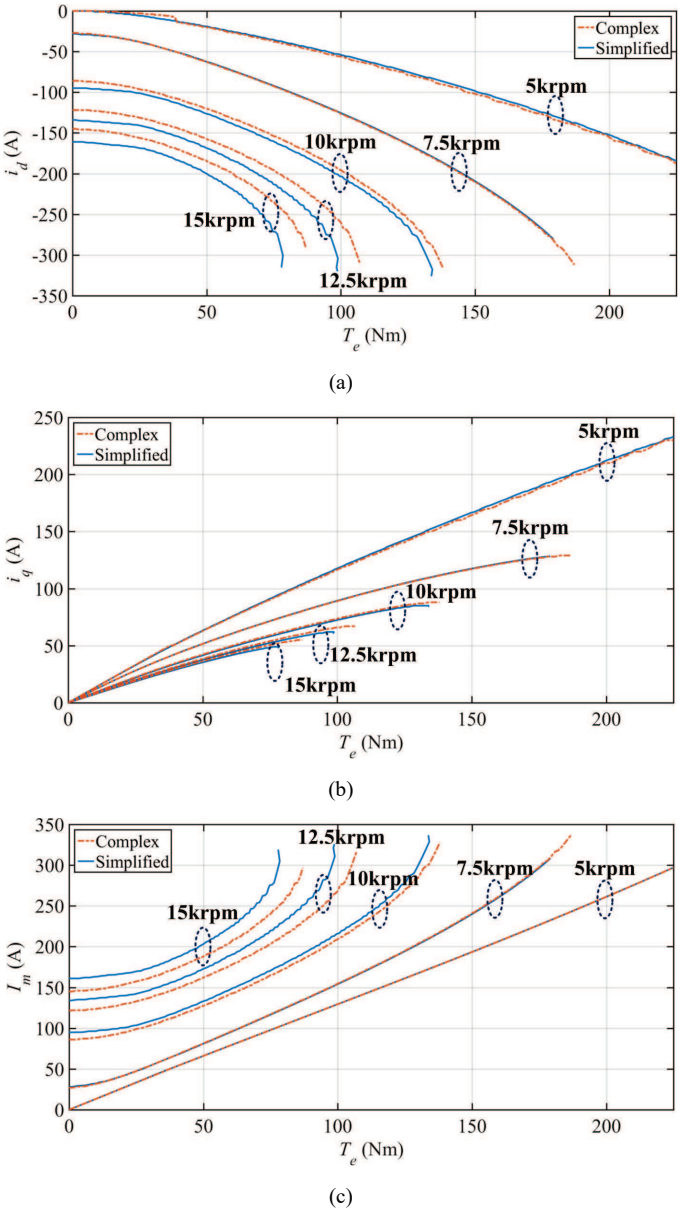

Fig. 11. Comparative study in term of current required for obtained torque-speed operation of tested IPM machine. (a) *d*-axis current. (b) *q*-axis current. (c) Current magnitude.

currents over obtained torques under the complex model and the simplified model without the activation of the voltage FB loop at 7500rpm and 10000rpm are respectively depicted in Figs. 9 and 10. Fig. 11 presents a comparative study between the complex model, Fig. 4, and simplified model, Fig. 8, for the tested IPM machine in terms of *dq*-axis currents and current magnitude over obtained torque-speed operations considering the aforementioned effects of the voltage FB loop in the FW operation region, Fig. 1(b). Also, relevant voltage magnitude under the complex and simplified models considering the effects of the voltage FB loop in the FW operation region are respectively depicted in Figs. 12(a) and 12(b). As can be seen, in the low-speed region (5000rpm) where MTPA operation is still implemented, although there are mismatches in *dq*-axis currents between the simplified model and the complex model

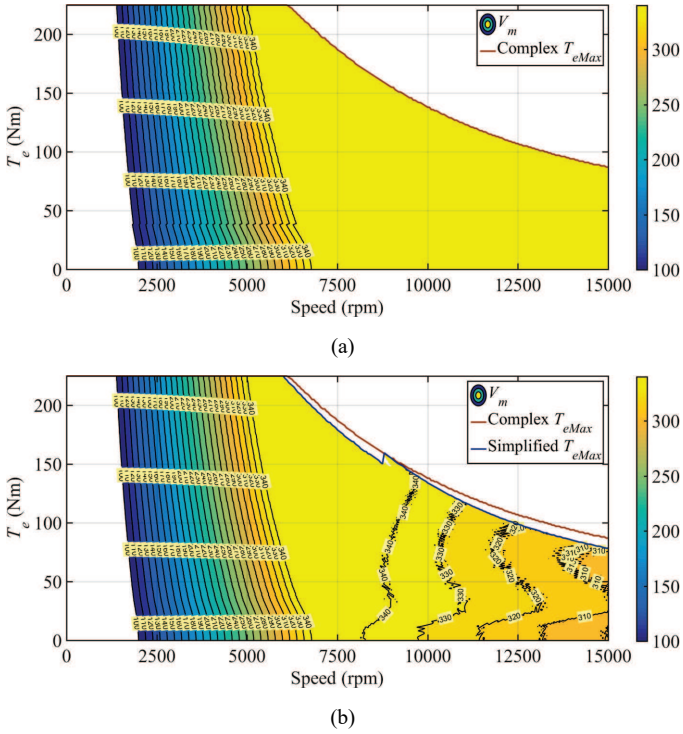

Fig. 12. Votage magnitude contour for obtained torque-speed operation of tested IPM machine. (a) Under complex model. (b) Under simplified model.

as shown in Figs. 11(a) and 11(b), the current magnitude for relevant obtained torque under the simplified model is very similar to the complex model, Fig. 11(c). This phenomenon could be explained by the fact that the segment around the MTPA operation point of the relevant constant torque over current magnitude curve are considerably flat and therefore, variation of *dq*-axis currents over these flat segments may not significantly affect the MTPA achievement for the obtained torque, Fig. 4(c). Similar phenomenon was introduced and discussed in details in [4]. As a result, MTPA control could be still achieved for the tested machine using the simplified model in the low-speed operation region (5000rpm), Fig. 11(c).

In the FW region, for a given obtained torque, the employments of non-ideal current reference LUTs may result in two main operation scenarios. The first operation scenario happens when the voltage magnitude is higher than the maximum achievable voltage value, $V_{\max}$. Fig. 9 illustrates this scenario for the tested IPM machine at 7500rpm under the simplified model together with the complex model of which machine voltage magnitude is well maintained at the $V_{\max}$ (346V), Fig. 9(a). As aforementioned, under this scenario, the voltage boundary could be maintained at the maximum achievable voltage value by the voltage FB loop via adjustment of *dq*-axis current references for a lower modulation index target, Fig. 1(b). By way of example, since its voltage magnitude is higher than the $V_{\max}$, the original operating point *a* for an obtained torque value as 140Nm in Fig. 9 will be adjusted vertically toward the operating point *c* by the voltage FB loop under the adjustment of current references from the targeted modulation index MI_1 toward the targeted modulation index MI_2, Fig. 1(b). However, when the adjusted operating

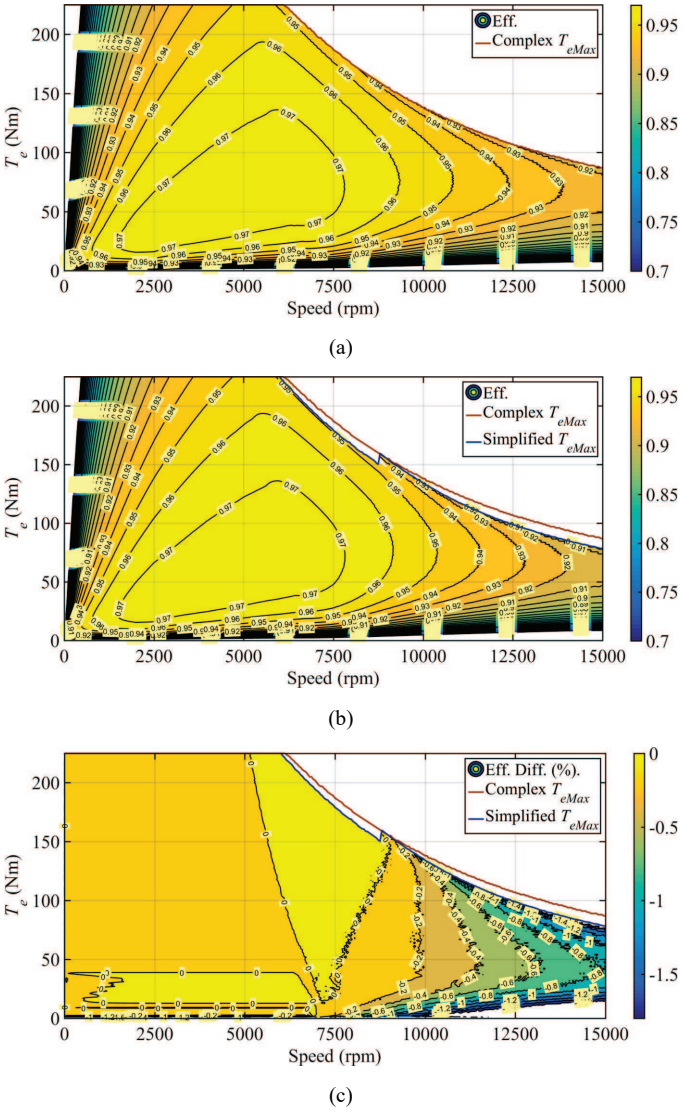

Fig. 13. Machine efficiency for obtained torque-speed operation of tested IPM machine. (a) Under complex model. (b) Under simplified model. (c) Efficiency difference.

point reaches to the operating point *b* in Fig. 9, its instantaneous voltage magnitude becomes equal to the V_{max} (346V), Fig. 9(a). Therefore, the operating point *b* is the new operating point for the obtained torque value as 140Nm under the simplified model considering the voltage FB loop adjustment. It is noted that the operating point *b* in Fig. 9 is also the relevant operating point for an obtained torque value as 140Nm under the complex model. Similar conclusions could be derived for all the operating points in Fig. 9 of which voltage magnitudes are higher the V_{max}. As a result, *dq*-axis currents, current magnitudes, and voltage magnitudes over obtained torques under this scenario for the simplified model are in agreement with the complex model. It is also noted that the voltage FB loop adjustment could compromise the maximum achievable torque, Fig. 1(d). The effects of the voltage FB loop adjustment could be obviously observed in Figs. 11 and 12 for *dq*-axis current, current magnitude, and voltage magnitude at 7500rpm over obtained torque values with acceptable agreement between the two models. However, a compromise on the maximum achievable torque is noticed for the simplified model, Fig. 12.

Also in the FW region with the simplified model, there is a second scenario where the machine voltage magnitude of a given obtained torque is lower than the maximum achievable voltage leading to the deactivation of the FB voltage loop. Fig. 10 depicts this scenario for the tested IPM machine at 10000rpm for the simplified model together with the complex model of which machine voltage magnitude is well maintained at the V_{max} (346V), Fig. 10(a). As can also be seen in Fig. 11(a), at higher speed FW operation (i.e., 12500rpm, and 15000rpm) the simplified model with non-ideal current reference LUTs may result in a higher than expected *d*-axis current for a given obtained torque leading to a lower than expected voltage magnitude, Figs. 10(a) and 12(b). Also, for a given obtained torque, with a higher than expected *d*-axis current, Figs. 10(b) and 11(a), a lower *q*-axis current compared with the complex model is required, Figs. 10(c) and 11(b). It is noted that since the obtained voltage magnitude in this scenario, Fig. 12(b), is lower than the maximum achievable voltage, Fig. 12(a), the MTPV control is not obtained leading to a higher than expected current magnitude for an obtained torque in comparison with the complex model, Fig. 11(c). As a result, a lower than expected machine efficiency is inevitable. In addition, a compromise on torque-speed boundary is also observed in Fig. 12(b) for the simplified model under this scenario. It is also noted that in practice, tested machine voltage is continuously varying as a function of machine temperature associated with selected cooling method and operation condition [17] and therefore, both the two operation scenarios may consecutively occur for a given torque-speed operation point.

On the other hand, machine efficiency under the complex and simplified models are respectively presented in Figs. 13(a) and 13(b). The efficiency difference over obtained torque-speed performance between the complex and simplified models is depicted in Fig. 13(c). Since MTPA operation could still be achieved for the simplified model, machine efficiencies under both complex and simplified models are highly similar for the low-speed region. In addition, machine efficiencies are also highly comparable for the two models in the FW region with first operation scenario where operated speed is around 7500rpm. However, in the FW region with second operation scenario where operated speed is higher than 10000rpm, implementation of the simplified model could result in a reduction up to 1.5% of machine efficiency, Fig. 13(c). It is noted that in terms of torque-speed performance, the simplified model could still maintain the expected torque-speed operation for the tested machine in the FW region with a reduction at the torque-speed boundary, Fig. 13(b).

Based on what have been discussed above, it is shown that the simplified model could be considered as a rapid solution to quickly test and validate magnetic design together with manufacture of the tested IPM traction machine with acceptable accuracy, especially at low-speed operation region. In the next section, measurement validations for the complex model and the simplified model are presented.

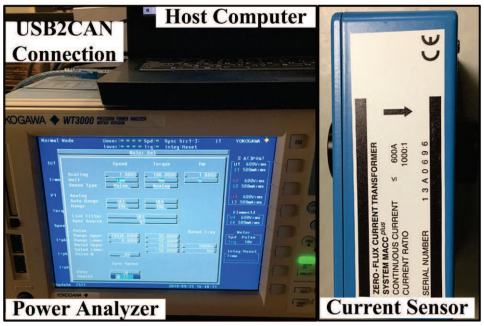

Fig. 14. Equipment for evaluation of complex and simplified model with tested IPM machine.

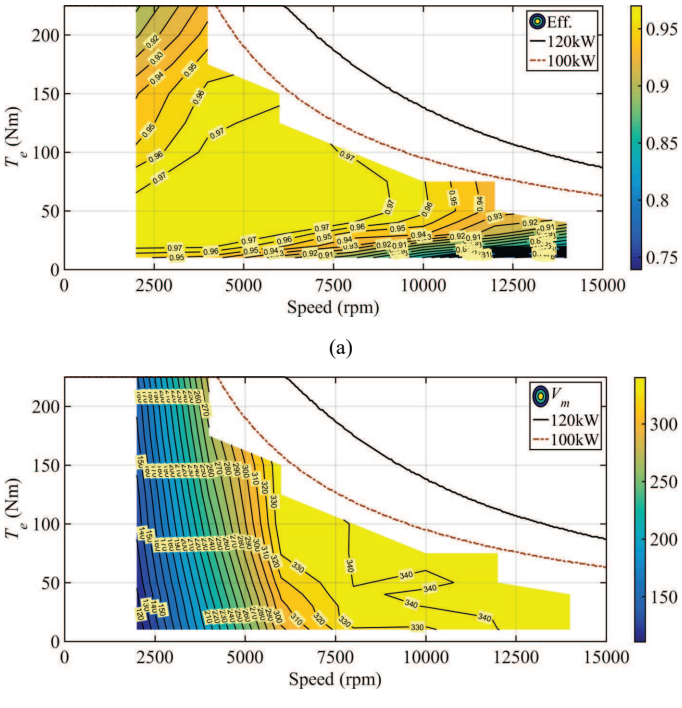

Fig. 15. Measured result of tested IPM machine under complex model. (a) Efficiency contour. (b) Voltage magnitude contour.

V. Experimental Results

To validate the capability of the simplified model as a rapid solution to quickly test and validate IPM machine design together with manufacture, both the complex-based current reference LUTs in Fig. 4 and the simplified-based current reference LUTs in Fig. 8 is respectively employed for testing the high-speed high-power (15000rpm, 120kW) IPM traction machine in Fig. 2(a) and machine efficiency over obtained torque-speed performance is measured and compared with the analysis result in Fig. 13. During the test, the dyno is operated under speed-control mode up to 14000rpm and the tested machine is controlled under torque-control mode by a high-voltage high-power (800Vdc, 300kW) inverter provided by an industry partner. A host-computer is used to regulate demanded torque of the employed inverter via CAN connection, Fig. 14. Under an operation speed, demanded torque up to the maximum achievable value is required for the tested IPM machine and a high-speed high-torque (20000rpm, 500Nm) torque transducer, KISTLER 4503B, is utilized to measure the actual obtained torque. Also, a high precision power analyzer Yokogawa WT3000 together with high accuracy current sensors MACC-

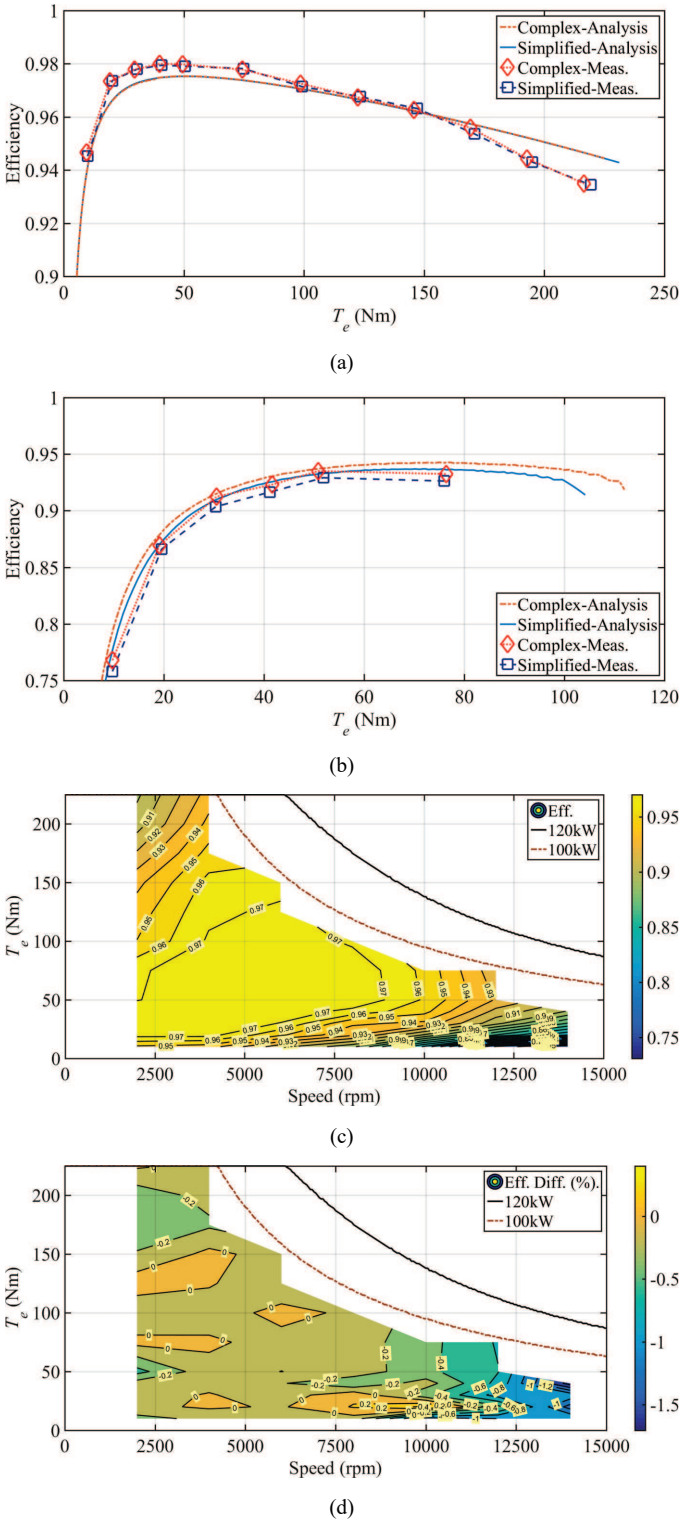

Fig. 16. Measured efficiency of tested IPM machine under simplified model. (a) Comparative study between analysis and measured results at 4000rpm. (b) Comparative study between analysis and measured results at 12000rpm. (c) Efficiency contour. (d) Efficiency difference between simplified and complex models.

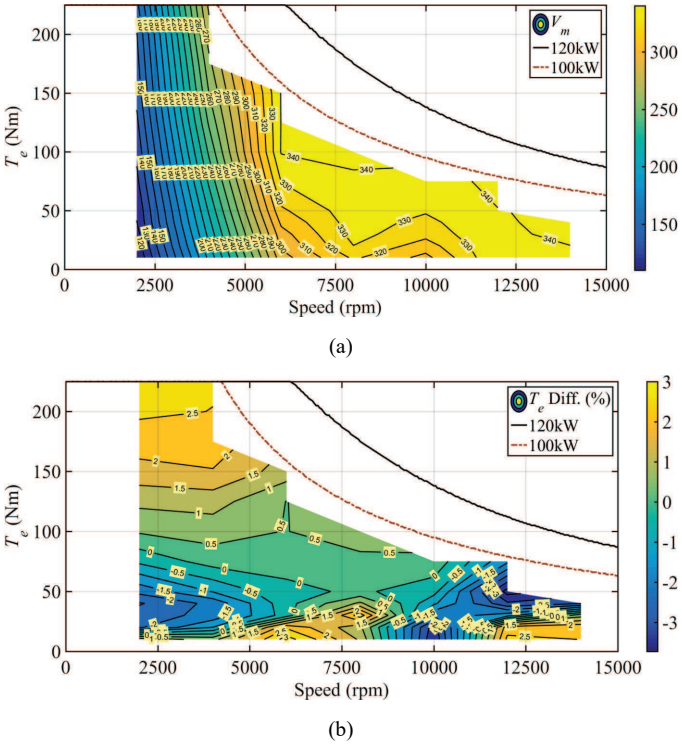

Fig. 17. Measured results of tested IPM machine under simplified model. (a) Voltage magnitude contour. (b). Torque difference contour.

plus are employed to measure the machine efficiency over obtained torque-speed performance, Fig. 14. To avoid performance instability in the FW operation region due to torque-speed boundary reduction under the simplified model as aforementioned, a scale down of maximum achievable power from 120kW to 100kW for the tested IPM machine is applied. It is noted that in the extreme high-torque/high-speed operation region, rotor temperature variation leading to compromising the tested IPM machine performance is inevitable [17].

Measurements of the tested machine under the complex model over obtained torque-speed performance is shown in Fig. 15 where a maximum efficiency torque-speed region higher than 97% could be achieved, Fig. 15(a). Also from Fig. 15(b), MTPV achievement could be observed for the tested machine in the high-speed/high-torque FW region with machine voltage magnitude is maintained around the $V_{\max}$ (346V). It is noted that measured efficiency map in Fig. 15(a) is in good agreement with the analysis results for the complex model in Fig. 13(a).

On the other hand, efficiency measurement of the tested machine under the simplified model over obtained torque-speed performance is presented in Fig. 16 where efficiency comparison between analysis and measured results at low-speed operation (4000rpm) under MTPA control and extreme high-speed operation (12000rpm) is respectively depicted in Figs. 16(a) and 16(b). As can be seen in Fig. 16(a), there is a good match in efficiency over operated torque at 4000rpm between the analysis and measured results. It is noted that due to the high temperature rise leading to the higher than expected winding copper losses in the high torque region [17], a difference up to 1% at the maximum peak-torque (225Nm) for the measured efficiency could be observed. Thus, MTPA

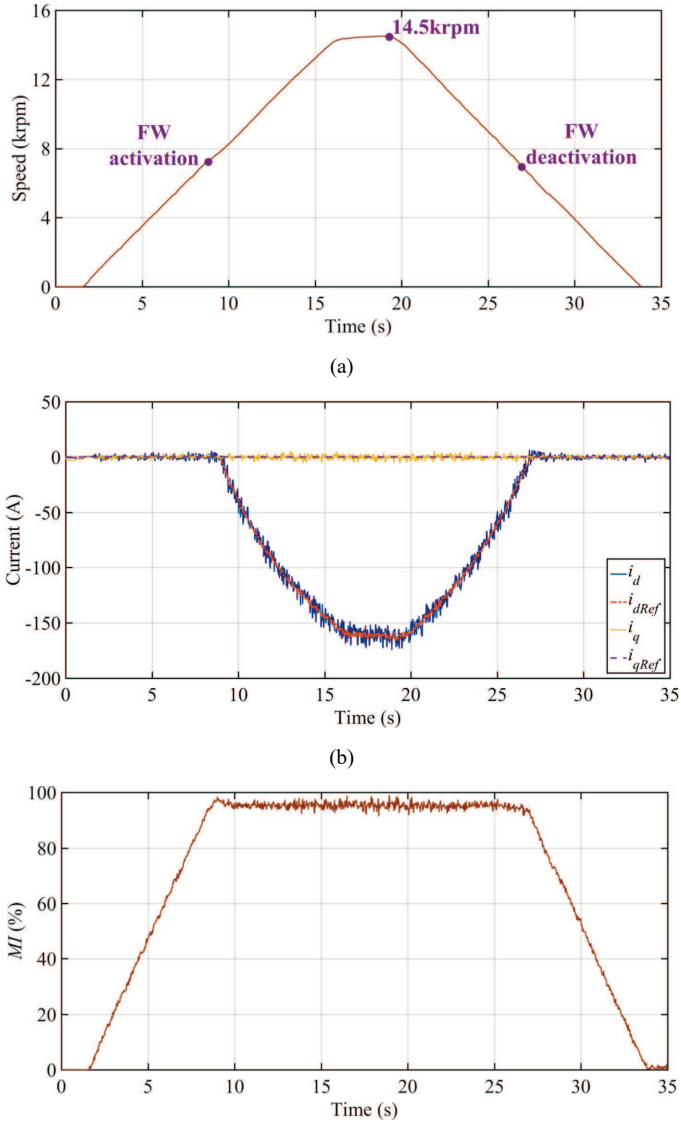

Fig. 18. Dynamic evaluation for tested IPM machine with simplified model. (a) Speed response. (b) *Dq*-axis currents. (c) Modulation index.

control could still be achieved for the simplified model. On the other hand, in the extreme high-speed operation region (12000rpm), around 1% efficiency difference is noticed for the measurement compared with the analysis result, Fig. 16(b). It is noted that in the extreme high-speed operation region, high temperature rise together with AC winding loss, windage loss, and bearing loss may cause unpredicted extra machine losses [17] and therefore the 1% efficiency difference at this extreme high-speed operation (12000rpm) between the analysis and measured results is highly acceptable.

Furthermore, measured efficiency map over obtained torque-speed performance for the tested machine is presented in Fig. 16(c) where a maximum efficiency torque-speed region higher than 97% could be achieved for the tested IPM traction machine with simplified control model and this maximum efficiency torque-speed region obtained is in good agreement with the measured result for the complex model, Fig. 15(a). In addition, measured efficiency map region over full torque-speed

performance in Fig. 16(c) is also well matched with the analysis result in Fig. 13(b). The difference of efficiency measurement over obtained torque-speed performance between the simplified and complex models is illustrated in Fig. 16(d). As can be seen, employment of the simplified model could provide very similar machine efficiency at low speed operation region up to about 10000rpm. At high-speed operation region, a difference efficiency up to 1.5% could be observed. It is noted that the measured result in Fig. 16(d) is in good agreement with the analysis result in Fig. 13(c).

To further demonstrate the simplified model, measured machine voltage magnitude over obtained torque-speed performance under the simplified model is presented in Fig. 17(a) where it is shown that machine voltage magnitude is well regulated around the peak voltage boundary (346V) in the FW operation region for the tested machine. Also, measured voltage contour in Fig. 17(a) is considerably agreed with the analysis result in Fig. 12(b). It is noted that machine voltage is continuously varying as a function of machine temperature associated with selected cooling method and operation condition [17]. Furthermore, the difference between demanded torque and actual obtained torque for the tested IPM machine with simplified model is illustrated in Fig. 17(b) where a maximum torque difference up to 3% could be achieved in the low-speed operation region. In the FW region, a maximum torque difference up to 4% could be observed.

In addition, dynamic evaluation for the tested IPM machine under the simplified model with a speed acceleration-deceleration up to 14500rpm is shown in Fig. 18. As can be seen, the FW operation is activated/deactivated at around 7000rpm and the modulation index is maintained around 94% (325V) in the high-speed operation region which is considerably matched with the analysis result in Fig. 12(b). It is worth noting that the good agreement between the measurement results in this section and the analysis result in the section IV highly demonstrates the capability of the simplified model as a rapid solution to quickly test and validate IPM machine design together with manufacture with acceptable accuracy, especially at low-speed operation region.

VI. Conclusions

The paper presents an evaluation on simplified model considering only effects of *q*-axis current on machine parameters for rapid identification and control development of IPM traction machines. The proposed simplified model is validated via measurement on a high-speed high-power (15000rpm, 120kW) IPM traction machine in both MTPA and FW operation regions. Based on the widely accepted assumption that the nonlinear characteristic of IPM traction machines is predominantly affected by the *q*-axis current, the simplified model proposed in the paper is equally applicable to other IPM traction machines (see the Appendix).

It is demonstrated that identification of the simplified model is simple, easy to be implemented, and could be quickly completed within a short-period of time. It is shown that in the low-speed operation region with MTPA control, due to the flat segment around the MTPA point of the relevant constant torque over current magnitude curve, MTPA operation could still be achieved for the tested machine with the simplified model. It is demonstrated that in the field-weakening (FW) region where effects of parameter mismatch resulting in a higher than expected voltage magnitude could be mitigated via a voltage FB loop, torque-speed performance could still be obtained for the tested machines under simplified model with a reduction in torque-speed boundary and up to 1.5% machine efficiency difference. Thus, the proposed simplified model can be considered at the earlier stages of identification and control development of IPM traction machine as a rapid solution to quickly test and validate machine design together with manufacture with acceptable accuracy, especially at low-speed operation region when full parameter validation is highly time-consuming.

Future work will include consideration of the simplified model as a rapid parameter identification and auto-tuning solution for IPM traction machines. Since torque-speed performance could still be obtained for the tested machine under the simplified model, the fine-tuning achievement could be attained later with online-adjusting technique.

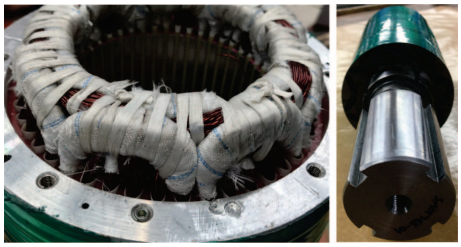

(a)

(b)

Fig. 19. Studied IPM traction machines. (a) Single-layer magnet rotor (main paper). (b) Double-layer magnet rotor (Appendix).

TABLE II

SPECIFICATIONS OF TESTED IPM MACHINE – DOUBLE-LAYER MAGNET ROTOR [4]

Continuous / Peak torque (Nm)	35 / 70
Peak current (A) / DC-link voltage (V)	125 / 120
Base / Maximum speed (rpm)	1200 / 4500
Number of pole pair	3

Appendix

For further demonstration of the simplified model, analysis results for a double-layer magnet rotor IPM traction machine, Fig. 19(b), of which specifications are presented in Table II/Fig. 20 and further details could be found in [4] are depicted in Figs.

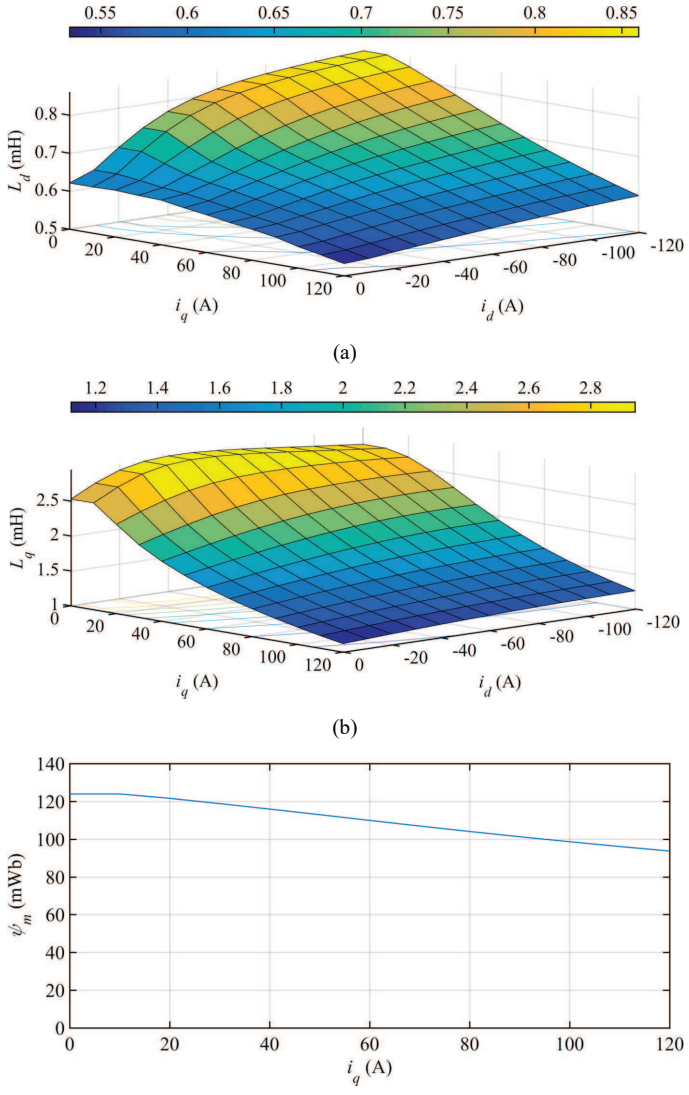

Fig. 20. Complex model of double-layer magnet rotor IPM machine, Fig. 19(b). (a) *d*-axis inductance. (b) *q*-axis inductance. (c) PM flux linkage.

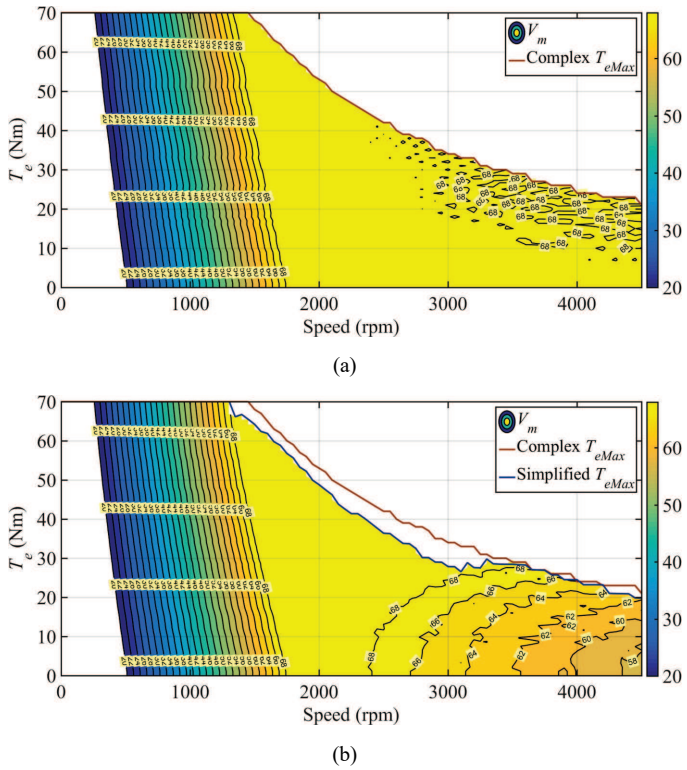

Fig. 21. Voltage magnitude contour for obtained torque-speed operation of double-layer magnet rotor IPM machine, Fig. 19(b). (a) Under complex model. (b) Under simplified model.

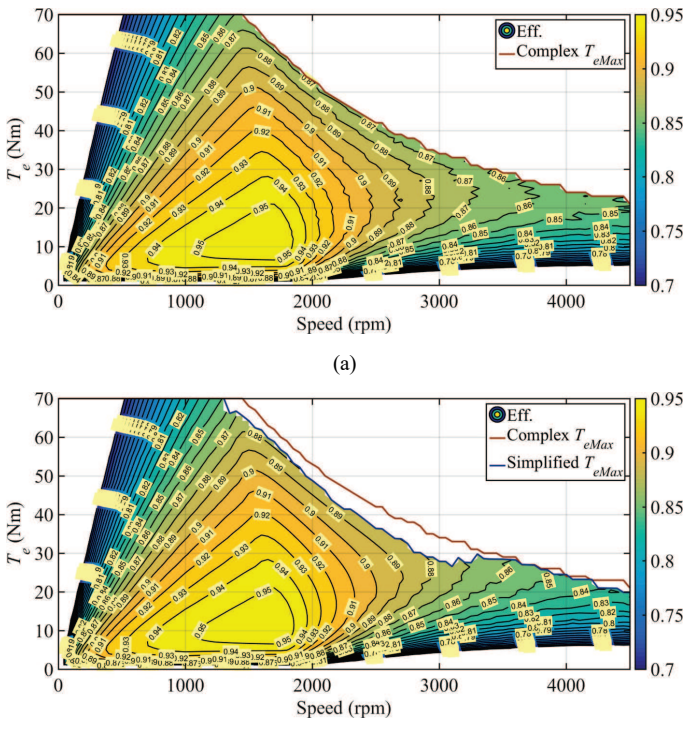

Fig. 22. Machine efficiency for obtained torque-speed operation of double-layer magnet rotor IPM machine, Fig. 19(b). (a) Under complex model. (b) Under simplified model.

21 and 22. As can be seen, similar conclusions as discussed in the main paper for the tested IPM machine with single-layer magnet rotor, Fig. 19(a), could also be obtained for the double-layer magnet rotor IPM machine controlled by the simplified model.

ACKNOWLEDGMENT

The authors would like to thank the anonymous reviewers for their valuable comments and suggestions that greatly contributed to improve the quality of this paper.

REFERENCES

[1] K. D. Hoang and K. Atallah, "A rapid concept development technique for electric vehicle power trains," *in Proc. IEEE Int. Conf. Connected Vehicles and Export (ICCVE) 2014*, Vienna, Austria, Nov. 3-7, 2014, pp. 191-198.

[2] M. Kamiya, "Development of traction drive motors for the Toyota hybrid systems," *IEEJ Trans. Ind. Appl.*, vol. 126, no. 4, pp. 473–479, Apr. 2006.

[3] K. D. Hoang, J. Wang, M. Cyriacks, A. Melkonyan and K. Kriegel, "Feed-forward torque control of interior permanent magnet brushless AC drive for traction applications," *in Proc. IEEE Int. Conf. Electric Mach. Drives (IEMDC) 2013*, Chicago, IL, US, pp. 152-159, 2013.

[4] K. D. Hoang and H. Aorith, "Online control of IPMSM drives for traction applications considering machine parameter and inverter nonlinearities,"

IEEE Trans. Transportation Electrification, vol. 1, no. 4, pp. 312-325, Dec. 2015.

[5] B. Stumberger, G. Stumberger, D. Dolinar, A. Hamler, and M. Trlep, "Evaluation of saturation and cross-magnetization effects in interior permanent magnet synchronous motor," *IEEE Trans. Ind. Appl.*, vol. 39, no. 5, pp. 1264–1271, Sep./Oct. 2003.

[6] K. M. Rahman and S. Hiti, "Identification of machine parameters of a synchronous machine," *IEEE Trans. Ind. Appl.*, vol. 41, no. 2, pp. 557–565, Mar./Apr. 2005.

[7] E. Armando, R. I. Bojoi, P. Guglielmi, G. Pellegrino, and M. Pastorelli, "Experimental identification of the magnetic model of synchronous machines," *IEEE Trans. Ind. Appl.*, vol. 49, no. 5, pp. 2116-2125, Sept.-Oct. 2013.

[8] S. A. Odhano *et al*., "Identification of three-phase IPM machine parameters using torque tests," *IEEE Trans. Ind. Appl.*, vol. 53, no. 3, pp. 1883-1891, May-June 2017.

[9] S. Hall, F. J. Márquez-Fernández and M. Alaküla, "Dynamic magnetic model identification of permanent magnet synchronous machines," *IEEE Trans. Energy Convers.*, vol. 32, no. 4, pp. 1367-1375, Dec. 2017.

[10] S. A. Odhano, P. Giangrande, R. I. Bojoi, and C. Gerada, "Self-commissioning of interior permanent magnet synchronous motor drives with high-frequency current injection," *IEEE Trans. Ind. Appl.*, vol. 50, no. 5, pp. 3295-3303, Sept.-Oct. 2014.

[11] S. A. Odhano, R. Bojoi, Ş. G. Roşu, and A. Tenconi, "Identification of the magnetic model of permanent-magnet synchronous machines using DC-biased low-frequency AC signal injection," *IEEE Trans. Ind. Appl.*, vol. 51, no. 4, pp. 3208-3215, July-Aug. 2015.

[12] K. D. Hoang, K. Atallah, J. Birchall, and S. Calverley, "Comparative evaluation of simplified and complex IPM machine model on control development of traction applications," in *Proc IEEE IECON'2019*, Lisbon, Portugal, 14 -17 Oct. 2019.

[13] H. Kim, Y. Lee, S. Sul, J. Yu, and J. Oh, "Online MTPA control of IPMSM based on robust numerical optimization technique," *IEEE Trans. Ind. Appl.*, vol. 55, no. 4, pp. 3736-3746, July-Aug. 2019.

[14] A. Rabiei, T. Thiringer, M. Alatalo, and E. A. Grunditz, "Improved maximum-torque-per-ampere algorithm accounting for core saturation, cross-coupling effect, and temperature for a PMSM intended for vehicular applications," *IEEE Trans. Transportation Electrification*, vol. 2, no. 2, pp. 150-159, June 2016.

[15] Y. Miao, H. Ge, M. Preindl, J. Ye, B. Cheng, and A. Emadi, "MTPA fitting and torque estimation technique based on a new flux-linkage model for interior-permanent-magnet synchronous machines," *IEEE Trans. Ind. Appl.*, vol. 53, no. 6, pp. 5451-5460, Nov.-Dec. 2017.

[16] B. Cheng and T. R. Tesch, "Torque feedforward control technique for permanent-magnet synchronous motors," *IEEE Trans. Ind. Electron.*, vol. 57, no. 3, pp. 969–974, Mar. 2010.

[17] K. D. Hoang, K. Atallah, P. Lazari, J. Birchall, and S. Calverley, "Thermal consideration on design and control development of IPM traction machines," in *Proc IEEE IECON'2019*, Lisbon, Portugal, 14 -17 Oct. 2019.

Khoa Dang Hoang (S'10-M'12-SM'19) received the B.Eng. and M.Sc.(Eng.) degrees from Ho Chi Minh City University of Technology (HCMUT), Ho Chi Minh City, Vietnam, in 2002 and 2005, respectively, and the Ph.D. degree from the University of Sheffield, Sheffield, United Kingdom, in 2011, all in electrical and electronics engineering.

From 2011 to 2019, he was a Research Associate in the Department of Electronic and Electrical Engineering, University of Sheffield, UK, where he is currently a Research and Development Engineer. His key research interests include power conversion, advanced control techniques for electrical drives, and analysis and design of electrical machines.

Panagiotis Lazari was born in Limassol, Cyprus, in 1986. He received the B.Eng. and Ph.D. degrees in Electrical Engineering from the University of Sheffield, UK.

From 2018 to 2020, he was a Research Associate in the Department of Electronic and Electrical Engineering, University of Sheffield, UK, where he is currently a member of Academic Staff at the Department of Multidisciplinary Engineering Education. His research interests include the design, multiphysics modelling and optimization of novel electrical machines for automotive and aerospace applications.

Kais Atallah received the Ingenieur d'Etat degree in electrical engineering from Ecole Nationale Polytechnique, El-Harrach, Algeria, 1988, and the Ph.D. degree from the University of Sheffield, Sheffield, U.K., in 1993. He is currently a Professor of Electrical Engineering with the University of Sheffield.

From 1993 to 2000, he was a Postdoctoral Research Associate with the Department of Electronic & Electrical Engineering, University of Sheffield. In 2006, he cofounded Magnomatics Ltd., where he was Director until July 2008. His research interests include fault-tolerant permanent magnet drives for safety-critical applications, magnetic gearing and "pseudo" direct drive electrical machines, and drive-trains for wind/tidal turbines and electrical/hybrid vehicles.

Jeff G. Birchall was born in U.K. in 1985. He received an M.Eng degree in Mechanical Engineering from University of Cambridge, UK, in 2009. Since joining Magnomatics Limited in 2010, he has become a Principal Engineer and is joint inventor of MAGSPLIT 2 and other related technologies in the field of magnetic gears.

Jeff enjoys system engineering considerations, optimization and design thinking for complex machines and problems across a wide range of industries and applications.

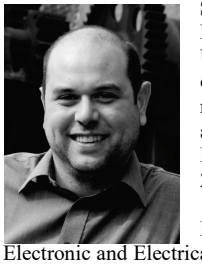

Stuart D. Calverley received the BEng degree in Mechanical Engineering from Loughborough University, Loughborough U.K. before moving to complete his PhD on "Design of a high speed switched reluctance machine for automotive turbo-generator applications" in the department of Electronic and Electrical Engineering at the University of Sheffield in 2001.

Following positions as a Royal Academy of Engineering Fellow and a lecturer in the department of Electronic and Electrical Engineering at the University of Sheffield, Sheffield, U. K. he co-founded Magnomatics Limited in 2006, where he is currently Chief Engineer. His activity includes the design and realization of electrical machines and magnetic gears for a wide range of applications, including large scale renewable generators, novel magnetic automotive hybrid transmission systems and high-performance motors for Autosport.